A Constrained Non-rigid Registration Algorithm for Use in Prostate Image-Guided Radiotherapy

W.H. Greene[1], S. Chelikani[2], K. Purushothaman[2], Z. Chen[3], J.P.S Knisely[3], L.H. Staib[1,2], X. Papademetris[1,2] and J. Duncan[1,2]

[1] Department of Biomedical Engineering,
[2] Department of Diagnostic Radiology
[3] Department of Therapeutic Radiology,
Yale University, New Haven, CT, USA
william.h.greene@yale.edu

Abstract. A constrained non-rigid registration (CNRR) algorithm for use in updating prostate external beam image-guided radiotherapy treatment plans is presented in this paper. The developed algorithm is based on a multi-resolution cubic B-spline FFD transformation and has been tested and verified using 3D CT images from 10 sets of real patient data acquired from 4 different patients on different treatment days. The registration can be constrained to any combination of the prostate, rectum, bladder, pelvis, left femur, and right femur. The CNRR was tested with 5 different combinations of constraints and each test significantly outperformed both rigid and non-rigid registration at aligning constrained bones and critical organs. The CNRR was then used to update the treatment plans to account for articulated, rigid bone motion and non-rigid organ deformation. Each updated treatment plan outperformed the original treatment plan by increasing radiation dosage to the prostate and lowering radiation dosage to the rectum and bladder.

1 Introduction

External-beam radiotherapy (EBRT) is one of the primary treatment modalities for prostate cancer [1]. Three-dimensional conformal radiotherapy (3DCRT) and intensity modulated radiotherapy (IMRT) have significantly increased the ability of EBRT to generate highly conformal radiation dose distributions for the prostate tumor volume with sharp dose falloff in the surrounding normal tissues. IMRT allows increased doses to be delivered to the prostate with acceptable acute and late toxicities for the nearby organs at risk, such as the rectum and bladder. However, when higher doses are to be delivered, precise and accurate targeting is essential because of unpredictable inter- and intra-fractional organ motions over the course of the daily treatments that often last more than seven weeks. Patient setup errors and internal organ motions must be taken into account in the treatment plan before dose-escalation trials are implemented in order to ensure accurate delivery of the planned dose to the prostate and to minimize the dose received by the rectum and bladder [2].

D. Metaxas et al. (Eds.): MICCAI 2008, Part I, LNCS 5241, pp. 780–788, 2008.

The latest advancement of Image-guided radiotherapy (IGRT) integrates an in-room cone-beam CT (CBCT) with radiotherapy linear accelerators for treatment day imaging. The CBCT images acquired on the treatment day enable the radiotherapist to rigidly adjust the position of the patient to best align the patient to the position used in the planning of the EBRT treatment. In addition to rigidly adjusting the position of the patient, a successful implementation of IGRT requires a robust non-rigid image registration and analysis technique to accurately align the patient anatomy on the treatment day to the patient anatomy on the planning day [3].

In this paper, we present a CNRR algorithm based on a multi-resolution cubic B-spline Free Form Deformation (FFD) transformation to capture the unpredictable articulated, rigid bone motion and internal organ deformation. The prostate, rectum, and bladder are used as non-rigid constraints and the pelvis, right femur, and left femur are used as rigid constraints. The constraint objects are independently registered prior to running the CNRR and the results are used in the CNRR to constrain the objects to their estimated position.

The transformation determined from the CNRR algorithm is used to update the planning day treatment plan to accurately account for bone and organ motion. An updated treatment plan that accurately accounts for bone and organ motion would allow for smaller planning margins and an escalated radiation dose, all while maintaining or lowering bladder and rectum toxicity levels [3][4].

2 Method

The CNRR algorithm consists of two steps. (**1**) Planning day organs {prostate, rectum, bladder} are independently registered to treatment day organs using a non-rigid transform. Planning day bones {pelvis, left femur, right femur} are independently registered to treatment day bones using a rigid transform. (**2**) The registration results are used to constrain the objects in the CNRR to their estimated transformations, generating $T_{0\to d}$, the transformation from the planning day image I_0 to the treatment day image I_d.

The estimated transformation $T_{0\to d}$ is used to update the planning day treatment plan P_0 to account for rigid bone motion and organ deformation, creating P_d, the updated treatment plan for treatment day d.

2.1 Independent Organ Registration

The segmented, binary prostate, rectum, and bladder images are independently registered using a non-rigid transform based on a multi-resolution cubic B-Spline FFD. A FFD based transform was chosen because a FFD is locally controllable due to the underlying mesh of control points which are used to manipulate the image [5].

A cubic B-spline FFD is defined by designating the image volume as $\Omega = \{(x, y, z)|0 \leq x < X, 0 \leq y < Y, 0 \leq z < Z\}$. Φ denotes a $(l+3)\times(m+3)\times(n+3)$ mesh of control points $\phi_{i,j,k}$ with uniform spacing $\delta_x, \delta_y, \delta_z = \delta$. The parameter

domain of the image is defined as $\Theta = \{(u,v,w)|0 \leq u \leq l, 0 \leq v \leq m, 0 \leq w \leq n\}$. The FFD can then be written as a 3D tensor product of 1D cubic B-splines

$$T_{0\to d}(x,y,z) = \sum_{i=0}^{3}\sum_{j=0}^{3}\sum_{k=0}^{3} B_i(u - \lfloor u \rfloor)B_j(v - \lfloor v \rfloor) \\ B_k(w - \lfloor w \rfloor)\phi_{(\lfloor u \rfloor + i)(\lfloor v \rfloor + j)(\lfloor w \rfloor + k)} \quad (1)$$

where $T_{0\to d}$ maps the planning day image I_0 to the treatment day image I_d, and $u = \frac{x}{\delta_x}, v = \frac{y}{\delta_y}, w = \frac{z}{\delta_z}$. In addition, B_i represents the i^{th} basis function of the cubic B-spline

$$B_0(u) = \tfrac{(1-u)^3}{6} \qquad B_2(u) = \tfrac{(-3u^3+3u^2+3u+1)}{6}$$

$$B_1(u) = \tfrac{(3u^3-6u^2+4)}{6} \quad B_3(u) = \tfrac{u^3}{6}.$$

The degree of non-rigid motion captured depends on the spacing of the control points in the mesh Φ. In order to create an algorithm with an adequate degree of non-rigid deformation, a hierarchical multi-resolution approach is implemented in which the control point resolution is increased in a coarse to fine fashion [6][7].

Let $\Phi^1, \Phi^2, \ldots, \Phi^N$ denote a hierarchy of control point meshes, each improving in resolution over the previous mesh. $T^1, T^2, \ldots, T^N$ are the transformations associated with each control point mesh. The composition of all transformations $\bar{T}(\Omega) = T^N \circ \cdots \circ T^2 \circ T^1(\Omega)$, is a map that defines the deformation of image volume Ω [6][7]. Thus, the transformation from the segmented planning day organ I_0^{obj} to the segmented treatment day organ I_d^{obj} is

$$\hat{\bar{T}}_{0\to d}^{obj}(x,y,z) = \hat{T}_{0\to d}^{obj-N} \circ \cdots \circ \hat{T}_{0\to d}^{obj-2} \circ \hat{T}_{0\to d}^{obj-1}(x,y,z). \quad (2)$$

In order to determine each individual transformation $\hat{T}_{0\to d}^{obj-n}$, we developed an objective function based on a sum of squared differences intensity matching term (C_{SSD}) and a transformation smoothing term (C_{smooth}).

The sum of squared differences intensity match function C_{SSD} is written as

$$C_{SSD}(T_{0\to d}(\Phi)) = \frac{1}{N}\sum_{i=0}^{N}\left[I_d(i) - I_0(T_{0\to d}(i,\Phi))\right]^2 \quad (3)$$

where i indexes over the voxels.

To ensure the transformation is smooth, each control point is restricted to move within a sphere of radius $r < R$, where $R \approx 0.4033 \times \delta$ [8][9][7]. The smoothing function is posed as

$$C_{smooth}(\Phi) = \sum_k f(\Phi_k) \quad (4)$$

where k indexes over the control points and

$$f(\Phi_k) = \begin{cases} 0 & \text{if } |\Phi_k| < 0.4033 \times \delta \\ |\Phi_k| & \text{otherwise} \end{cases}.$$

Each individual transformation $\hat{T}_{0\to d}^{obj-n}$ in (2) is estimated by using a conjugate gradient optimizer to minimize the following objective function with respect to $T_{0\to d}^{obj-n}$

$$\hat{T}_{0\to d}^{obj-n} = \arg\min_{T_{0\to d}^{obj-n}} \left[C_{SSD}(T_{0\to d}^{obj-n}(\Phi^{obj-n})) + C_{smooth}(\Phi^{obj-n}) \right]. \quad (5)$$

The control point mesh Φ^{obj-n} is used as a constraint in the CNRR.

2.2 Independent Bone Registration

The segmented, binary pelvis, left femur and right femur images are independently registered using a rigid transformation to find the optimal $\hat{\hat{T}}_{0\to d}^{r,obj}$ which maps I_0^{obj} into I_d^{obj}

$$\hat{\hat{T}}_{0\to d}^{r,obj}(x,y,z) = \hat{T}_{0\to d}^{r,obj-N} \circ \cdots \circ \hat{T}_{0\to d}^{r,obj-2} \circ \hat{T}_{0\to d}^{r,obj-1}(x,y,z). \quad (6)$$

To estimate each $\hat{T}_{0\to d}^{r,obj-n}$, we minimize C_{SSD} with respect to $T_{0\to d}^{r,obj-n}$ using a conjugate gradient optimizer

$$\hat{T}_{0\to d}^{r,obj-n} = \arg\min_{T_{0\to d}^{r,obj-n}} C_{SSD}(T_{0\to d}^{obj-n}). \quad (7)$$

Each rigid transformation $\hat{T}_{0\to d}^{r,obj-n}$ is applied to an associated control point mesh Φ^{obj-n}, which is used as a constraint in the CNRR.

2.3 Constrained Non-rigid Registration

The constrained non-rigid registration algorithm uses the same FFD transform developed in Sec. 2.1 to estimate the optimal $\hat{\hat{T}}_{0\to d}$ which maps the planning day image I_0 into the treatment day image I_d.

$$\hat{\hat{T}}_{0\to d}(x,y,z) = \hat{T}_{0\to d}^{N} \circ \cdots \circ \hat{T}_{0\to d}^{2} \circ \hat{T}_{0\to d}^{1}(x,y,z) \quad (8)$$

To estimate each $\hat{T}_{0\to d}^{n}$, we developed a cost function based on C_{SSD}, C_{smooth}, and an object matching function (C_{object}).

The object matching function C_{object} aligns the organs and bones by forcing the control points that lie within the segmented objects to their position estimated by the individual object registration.

$$C_{object}(\Phi^n) = \sum_{obj} \sum_{k\in obj} \left[\Phi_k^n - \Phi_k^{n-obj} \right]^2 \quad (9)$$

where k indexes over the control points and obj indexes over any combination of constraint objects {prostate, rectum, bladder, pelvis, right femur, left femur} used in the registration.

Each $\hat{T}^n_{0\to d}$ in (8) is estimated using a conjugate gradient optimizer to minimize the following objective function using weight α with respect to $T^n_{0\to d}$

$$\hat{T}^n_{0\to d} = \arg\min_{T^n_{0\to d}} \left[C_{SSD}(T^n_{0\to d}(\Phi^n)) + \alpha C_{object}(\Phi^n) + \alpha C_{smooth}(\Phi^n)\right]. \quad (10)$$

2.4 Updating and Assessing the Treatment Plan

The dose distributions in the tumor and organs at risk are analyzed by using the dose volume histogram (DVH), which plots the dose distribution throughout the organs (prostate, rectum, bladder). The prostate DVH can be reduced to a single metric known as the tumor control probability (TCP) and the normal tissue DVH can be reduced to the normal tissue complication probability (NTCP), which is calculated for both the rectum and bladder [10][11]. An optimal treatment plan maximizes the TCP while minimizing both rectal and bladder NTCP.

The treatment day TCP and NTCP values are calculated using the planning day treatment plan P_0 and treatment day image I_d and compared to the planning day values calculated using P_0 and I_0. If the treatment day NTCP for a healthy organ is greater than the planning day NTCP, then that organ is used as a constraint in the CNRR. The prostate is always used as a constraint. The transformation estimated from the CNRR result is used to warp P_0 into P_d, the updated treatment plan for day d.

3 Results

We used ten sets of real patient data acquired from four different patients. Two patients each had three treatment day CT images, and an additional two patients each had two treatment day CT images. Each of the four patients analyzed had an associated planning day 3DCRT treatment plan and CT image. The images and treatment plans were re-sliced to a clinically applicable spatial resolution of $4mm \times 4mm \times 4mm$. The prostate, rectum, and bladder were hand segmented by a qualified clinician. The pelvis, left femur, and right femur were segmented using *BioImage Suite* [12].

The CNRR was tested for robustness using 5 different constraint scenarios (Table 1); The weighting factor in (10) was set to infinity. The treatment plans were then updated by selecting registration constraints as described in Sec. 2.4. Registration and treatment plan results are presented below.

3.1 Registration Results

The CNRR algorithm was tested using 5 different constraint scenarios (Table 1) to determine how the constrained organs and bones affected the transformation of the unconstrained organs and bones. The control point spacing started at

Table 1. Registration Tests

Test	# Constraints	Objects Constrained
NRR	0	None – Non-Rigid Registration
CNRR-1	1	Prostate
CNRR-2	2	Bladder, Prostate
CNRR-3	3	Pelvis, L. Femur, R. Femur
CNRR-5	5	Pelvis, L. Femur, R. Femur, Bladder, Prostate
CNRR-6	6	Pelvis, L. Femur, R. Femur, Bladder, Rectum, Prostate

$\delta = 25mm$ and was refined to $\delta = 14mm$ over 10 iterations. For comparison, a non-rigid registration (NRR) and rigid registration (RR) were performed on all ten sets of real patient data. Object overlap was tracked at each iteration of the registration and was used as a metric to assess the quality of the registration and the improvement generated at each iteration.

The RR performed the poorest out of all the registrations algorithms, generating an identity transform for all ten sets of patient data. The RR results are not discussed further.

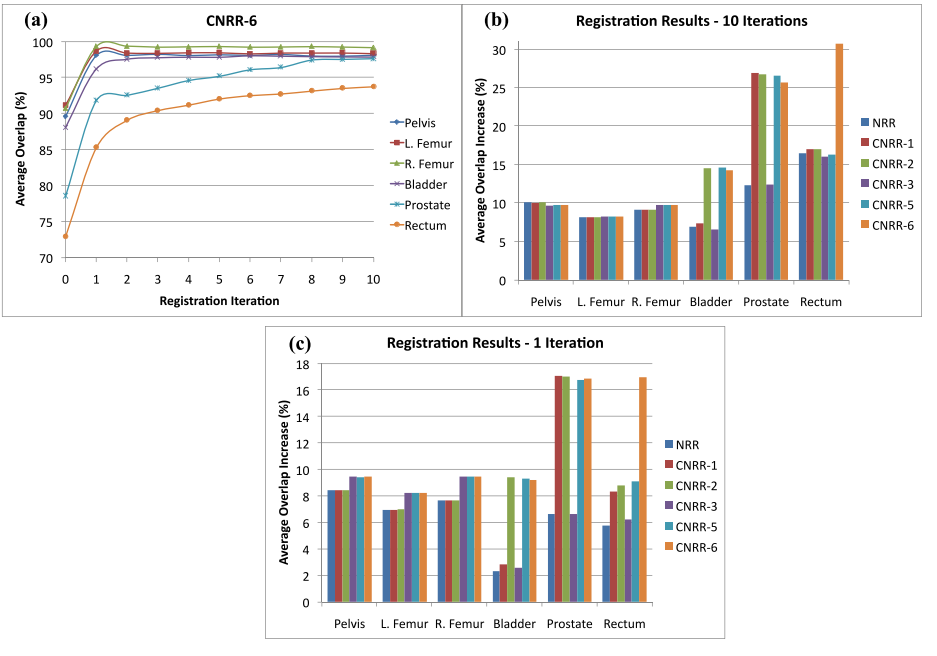

Fig. 1. Registration results presented are averaged over 10 sets of real patient data acquired from 4 different patients. (a) Average object overlap results at each iteration of CNRR-6, where iteration '0' represents the initial object overlap. (b) Average object overlap increase achieved after 10 iterations. Results are from NRR and 5 CNRR tests performed. (c) Average object overlap increase achieved after 1 iteration. Results are from NRR and 5 CNRR tests performed. For each object, more than 40% of the overlap increase acquired after 10 iterations was achieved in the first iteration.

The CNRR significantly outperformed the NRR at aligning constrained organs and bones. The overlap increase for each object after 10 iterations is presented in Fig. 1b. The best overlap results were generated when all 6 objects were used as constraints in CNRR-6 (Fig 1a). The most significant object overlap gains were made in the first registration iteration (Fig. 1c). The results indicate that constrained objects did not improve the overlap of unconstrained objects. All results presented in Fig. 1 are averaged over the ten sets of real patient data.

3.2 Treatment Plan Results

All four 3DCRT treatment plans were updated for each associated treatment day CT image. Due to set-up errors, inter- and intra-organ motion, treatment plan results varied from patient to patient and day to day. For this reason, results must be presented on an individual and daily basis.

As an example, normalized results from two treatment days for patient 2 are presented in Fig. 2. On both treatment days, the TCP and bladder NTCP were poorer than the planning values, so only the prostate and bladder were used as constraints. We tested three constraint scenarios, CNRR-1,2,5, with 10 iterations each. The best results occurred when both the prostate and bladder were held as constraints (CNRR-2). For both days, the TCP value did not decrease much from the planning TCP value due to the large planning margins used in 3DCRT that ensure the prostate receives the complete dose of radiation, so little correction was observed. However, updating the treatment plan significantly decreased bladder NTCP for all constraint scenarios tested. Including the bones as constraints in addition to the prostate and bladder (CNRR-5) did not further

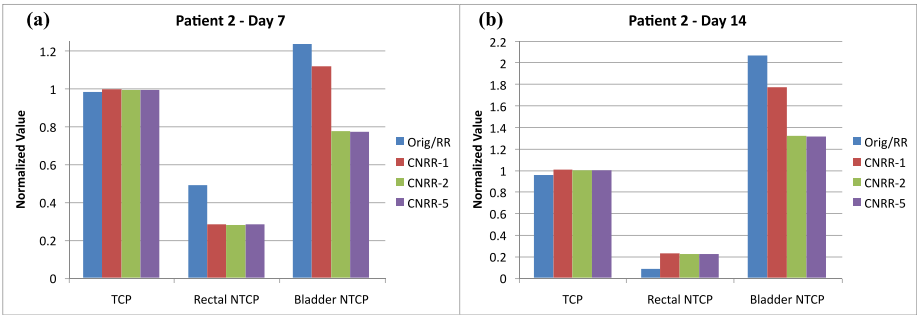

Fig. 2. TCP, NTCP Results for Patient 2 acquired from original and updated treatment plans. Results normalized by dividing treatment day value by planning day value. Original treatment plan was updated using RR, CNRR-1,2,5. For both days, CNRR-1,2,5 increased TCP and decreased bladder NTCP. CNRR-2,5 decreased bladder NTCP the most due to the bladder constraint. Bone constraints in CNRR-5 did not improve values when compared to CNRR-2. (a) Day 7 results. CNRR-1,2,5 improved rectal NTCP. (b) Day 14 results. Rectal NTCP was slightly increased in CNRR-1,2,5.

improve treatment plan results when compared to those with just the prostate and bladder (CNRR-2).

4 Discussion

For each patient and constraint combination tested, the CNRR proved to be highly robust and significantly improved the overlap for each constrained object and outperformed the results achieved from the RR and NRR.

Updating each treatment plan to account for prostate deformation and motion slightly improved the treatment day TCP for each patient. Although the treatment day TCP did not decrease much in each case due to the large planning margins used around the prostate in 3DCRT plans, nominal TCP improvements were achieved. Had IMRT plans, which provide more highly conformal and smaller dose planning margins, been used, significant improvements in the TCP would have been achieved.

Updating the treatment plans to improve the treatment day NTCP for normal organs significantly lowered the NTCP for these organs. When used to update the treatment plan, the CNRR transformation pulled the low radiation areas that were initially planned in the healthy organs back into the organs, improving the NTCP.

While the updated treatment plans may not be immediately realized without making corresponding modifications to the treatment beams, the updated plan will (**1**) serve as the new dose prescription for optimizing the fluence map of the treatment beams so that the updated plan can be physically delivered or (**2**) serve as a guide so that a closely matched realizable plan, selected from a library of preapproved plans, can be used to deliver the updated dose distribution. While the first approach would be ideal, it is not clinically feasible due to time constraints. The latter approach, however, is time efficient and can be implemented clinically.

References

1. Potosky, A.L., Legler, J., Albertsen, P.C., Stanford, J.L., Gilliland, F.D., Hamilton, A.S., Eley, J.W., Stephenson, R.A., Harlan, L.C.: Health outcomes after prostatectomy or radiotherapy for prostate cancer: Results from the prostate cancer outcomes study. J. Nat. Cancer Inst. 92, 1582–1592 (2000)
2. Ghilezan, M., Yan, D., Liang, J., Jaffray, D., Wong, J., Martinez, A.: Online imageguided intensity-modulated radiotherapy for prostate cancer: How much improvement can we expect? A theoretical assessment of clinical benefits and potential dose escalation by improving precision and accuracy of radiation delivery. Int. J. Radiation Oncology Biol. Phys. 60(5), 1602–1610 (2004)
3. Dawson, L.A., Sharpe, M.B.: Image-guided radiotherapy: rationale, benefits, and limitations. Lancet. Oncol. 7, 848–858 (2006)
4. Klein, E.E., Drzymala, R.E., Purdy, J.A., Michalski, J.: Errors in radiation oncology: a study in pathways and dosimetric impact. J. Appl. Clin. Med. Phys. 62, 1517–1524 (2005)

5. Rogers, D.: An Introduction to NURBS: with Historical Perspective, 1st edn. Morgan Kaufmann Publishers, San Francisco (2001)
6. Rueckert, D., Sonoda, L., Denton, E., Rankin, S., Hayes, C., Leach, M.O., Hill, D., Hawkes, D.J.: Comparison and evaluation of rigid and non-rigid registration of breast MR images. In: SPIE, vol. 3661, pp. 78–88 (1999)
7. Greene, W.H., Chelikani, S., Papademetris, X., Knisely, J.P.S., Duncan, J.: A constrained non-rigid registration algorithm for application in prostate radiotherapy. In: ISBI, pp. 740–743 (April 2007)
8. Choi, Y., Lee, S.: Local injectivity conditions of 2D and 3D uniform cubic b-spline functions. In: Proc. of Pacific Graphics, pp. 302–311 (1999)
9. Rueckert, D., Aljabar, P., Heckemann, R., Hajnal, J.V., Hammers, A.: Diffeomorphic registration using b-splines. In: Larsen, R., Nielsen, M., Sporring, J. (eds.) MICCAI 2006. LNCS, vol. 4191, pp. 702–709. Springer, Heidelberg (2006)
10. Cozzi, L., Buffa, F.M., Fogliata, A.: Comparative analysis of dose volume histogram reduction algorithms for normal tissue complication probability calculations. Acta Oncologica. 39(2), 165–171 (2000)
11. Kutcher, G.J., Burman, C., Brewster, L., Goitein, M., Mohan, R.: Histogram reduction method for calculating complication probabilities for three-dimensional treatment planing evaluations. Int. J. Radiation Oncology Biol. Phys. (21), 137–146 (1991)
12. Papademetris, X., Jackowski, M., Rajeevan, N., Constable, R., Staib, L.: BioImage Suite: An integrated medical image analysis suite, Section of Bioimaging Sciences, Dept. of Diagnostic Radiology, Yale School of Medicine, `http://www.bioimagesuite.org`